

Shem: A Hardware-Aware Optimization Framework for Analog Computing Systems

Yu-Neng Wang
wynwyn@stanford.edu
Stanford University
USA

Sara Achour
sachour@stanford.edu
Stanford University
USA

Abstract

As the demand for efficient data processing escalates, reconfigurable analog hardware which implements novel analog compute paradigms, is promising for energy-efficient computing at the sensing and actuation boundaries. These analog computing platforms embed information in physical properties and then use the physics of materials, devices, and circuits to perform computation. These hardware platforms are more sensitive to nonidealities, such as noise and fabrication variations, than their digital counterparts and accrue high resource costs when programmable elements are introduced. Identifying resource-efficient analog system designs that mitigate these nonidealities is done manually today.

While design optimization frameworks have been enormously successful in other fields, such as photonics, they typically either target linear dynamical systems that have closed-form solutions or target a specific differential equation system and then derive the solution through hand analysis. In both cases, time-domain simulation is no longer needed to predict hardware behavior. In contrast, described analog hardware platforms have nonlinear time-evolving dynamics that vary substantially from design to design, lack closed-form solutions, and require the optimizer to consider time explicitly. We present Shem, an optimization framework for analog systems. Shem leverages differentiation methods recently popularized to train neural ODEs to enable the optimization of analog systems that exhibit nonlinear dynamics, noise and mismatch, and discrete behavior. We evaluate Shem on oscillator-based pattern recognizer, CNN edge detector, and transmission-line security primitive design case studies and demonstrate it can improve designs. To our knowledge, the latter two design problems have not been optimized with automated methods before.

1 Introduction

There has been an emergence of new workloads that place extreme power constraints on the hardware and require processing near the sensing and actuation interfaces [4, 32, 42, 59]. Analog computing systems are a promising class of hardware that can perform processing directly on analog signals domain and often at very low energy, enabling processing large amounts of analog data with little digitization [1, 57]. Analog computing systems encode information in physical

signals (e.g., voltage) and then leverage the dynamics of materials, devices, and circuits to perform computation. Modern analog computing systems are reconfigurable and implement novel analog computational paradigms, such as oscillator-based computing and cellular nonlinear networks, which are inherently nonlinear and often use non-standard physical properties [24, 39, 54, 63, 64]. Ordinary differential equations capture the semantics of the analog compute paradigm and executing computations involves solving or simulating the differential equation system.

Design Challenges. Identifying a resource-efficient, system-level design for this class of analog hardware that delivers acceptable fidelity remains a significant challenge and is primarily performed manually. First, analog hardware is sensitive to *nonidealities* that affect the fidelity of the computation, such as noise, fabrication-induced parameter variations, and environmental sensitivities. Second, the digital interface circuitry used to program the hardware and perform digital/analog conversion increases resource usage, especially with increasing precision [2, 15, 26, 29, 68]. Reducing the precision of these digital elements and the degree of programmability significantly reduces the complexity of the design. *Enabling automated optimization of these analog systems would enable identification of useful design.*

1.1 Existing Design Optimization Methods

Design optimization tools find design parameterizations that minimize some *cost function*, which captures the end-to-end system-level property the designer desires. Gradient-based optimization methods have been extensively used in photonics [30, 47, 48, 55, 55, 66]. Because these optimizers use gradient information to drive the search intelligently and are built on heavily accelerated ML frameworks, designs of tens or even hundreds of thousands of design variables can be targeted [35, 60]. Gradient-based optimizers have also been used to optimize analog circuits to a lesser degree; these methods optimize SPICE circuits to minimize specific circuit metrics (e.g., delay) and typically leverage optimization techniques that specifically work with circuit schematics [13, 14, 19, 28, 34, 45, 62, 69].

Limitations. The gradient-based methods devised in these prior works are insufficient for optimizing analog computing systems. To be able to use these methods, the gradient of the cost function must be taken. Previously developed

optimizers primarily target linear dynamical systems that have closed-form solutions or target a specific differential equation system that has a hand-derived solution. In both cases, time-domain simulation is no longer needed to predict hardware behavior, and the gradient is relatively straightforward to compute. In contrast, this class of analog systems has nonlinear dynamics that rarely have analytic solutions, so gradient needs to be taken over the time domain simulation of the system.

Analog systems also experience nonidealities, such as fabrication-induced errors and noise that introduce stochasticity into the system’s dynamics. This stochastic behavior is not inherently differentiable and interacts with the system’s nonlinearities, producing complex behaviors. In addition, digital logic that exists at the programming and measurement interfaces of the analog system is inherently discrete and, therefore, also not readily differentiable. These behaviors make the system even more challenging to differentiate.

1.2 Optimization of Analog Systems with Shem

We present Shem, an optimization framework for analog systems that directly optimizes over time-domain differential equation models with nonlinear dynamics. Shem leverages the adjoint method, a differentiation method recently popularized to train neural ODEs, to directly differentiate over ordinary differential equation simulations and find the gradient of the cost function [8, 36, 46]. Shem deploys a translation pass that makes noise, mismatch, and digital logic differentiable so the gradient may be taken.

We build Shem on the JAX machine learning framework, which supports auto-differentiation and offers highly optimized backends for auto-parallelization and hardware acceleration, enabling scalable design optimization [5]. Shem inherits the programming conveniences offered by JAX, enabling Shem to target a range of analog system designs and optimize complex cost functions that evaluate system-level properties such as end-to-end error.

1.2.1 Contributions.

- We introduce techniques that enable time-domain design optimization of analog systems and differentiation over noise, fabrication variations, and digital logic.
- We present Shem, a framework built on JAX that supports auto-differentiation and optimization of nonlinear time-domain analog systems.
- We evaluate Shem on oscillator-based pattern recognizer, cellular nonlinear network edge detector, and transmission-line security primitive design case studies and demonstrate it can improve designs. To our knowledge, the latter two design problems have not been optimized with automated methods before.

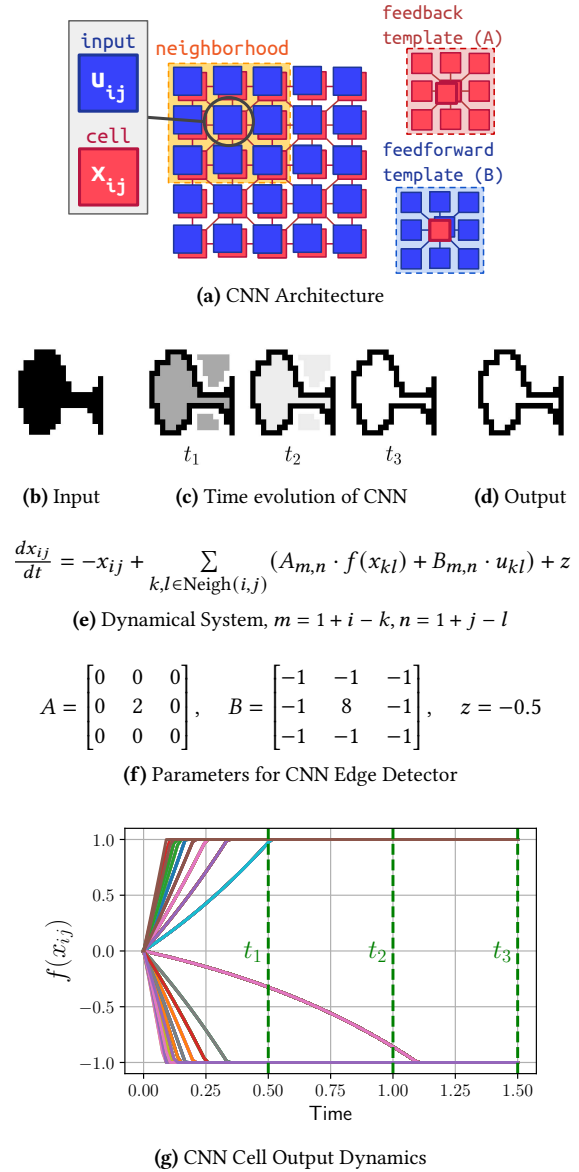


Figure 1. Cellular Nonlinear Network Edge Detector.

2 Example: CNN Edge Detector

Let us first consider a cellular nonlinear network-based implementation of an edge detector. A cellular nonlinear network (CNN) is an analog compute paradigm that has applications in image processing, partial differential equation (PDE) solving, and security primitives [10, 12, 17, 23].

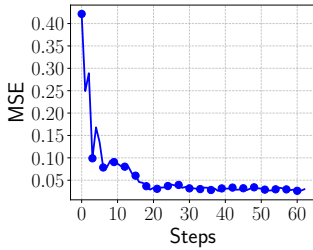
Overview. A CNN consists of a grid of locally interconnected cells with values that evolve over time. Figure 1a presents a visualization of the CNN; the nodes map to cells, and edges capture interactions between cells. Each cell at row i column j has a *state variable* x_{ij} that evolves over time, associated external input u_{ij} , and is connected to a neighborhood of cells. In the CNN edge detector application, each external

$$\frac{dx_{ij}}{dt} = -x_{ij} + \sum_{k,l \in \text{Neigh}(i,j)} (\delta_{i,j,k,l}^A \cdot A_{m,n} \cdot f(x_{kl}) + \delta_{i,j,k,l}^B \cdot B_{m,n} \cdot u_{kl}) + \delta_{i,j}^z \cdot z$$

(a) Dynamical System, $m = 1 + i - k, n = 1 + j - l$



(b) No Optimization ($loss = 0.555$). (c) W/ Optimization ($loss = 0.032$).



(d) Loss over Optimizer Iterations

$$A = \begin{bmatrix} -0.37 & 0.68 & -0.37 \\ 0.68 & 0.60 & 0.68 \\ -0.37 & 0.68 & -0.37 \end{bmatrix}$$

$$B = \begin{bmatrix} -1.21 & -0.68 & -1.21 \\ -0.68 & 7.76 & -0.68 \\ -1.21 & -0.68 & -1.21 \end{bmatrix}$$

$$z = -1.77.$$

(e) Optimized Parameters

Figure 2. Optimizing CNN edge detector with device mismatch. Initial loss 0.042, optimized loss 0.027.

input u_{ij} maps to the greyscale pixel value at position i, j of the image input, and the state variable $x_{i,j}$ settles to the edge detector value. Figure 1b shows the input image provided with external inputs $u_{i,j}$, and Figures 1c and 1d, respectively, show the evolution of cell outputs over time and the final cell output value. We can see from Figure 1d that the CNN edge detector cells on the borders of the shape settle to black.

Differential Equation Model. The dynamics of each state variable x_{ij} is modeled with an ordinary differential equation (ODE), which captures the evolution of the cell’s value over time. Figure 1e presents the ordinary differential equation for cell x_{ij} of the CNN. The derivative of each cell’s state x_{ij} is determined by the states of other cells x and external inputs u . The state of each cell undergoes a nonlinear activation function f . In CNN edge detection, the activation function f clamps the input to the range $[-1, 1]$.

Parameters. The parameter configuration programs the CNN to perform the edge detection. The feedback template A determines how the neighboring cells’ values contribute to a given cell, and the feedforward template B determines how the neighboring external input values contribute to a given cell. The parameter z offsets the cell’s value. Figure 1f presents the A template, B template, and z parameter instantiation for the CNN edge detector [11, 20, 44].

Simulation. We obtain the output of the CNN edge detector by simulating the differential equations that govern the system over time. Figure 1g shows the cell’s output traces over

time. Each external input $u_{i,j}$ is set to the pixel values at i, j , the cells $x_{i,j}$ are instantiated to zero, and then the dynamical system is simulated over time using a differential equation solver. The edge detector pixel value at a pixel location i, j is measured from the CNN by applying the activation function $f(\cdot)$ to each cell’s value. The CNN dynamics have a transient phase of execution where the output pixel values are in flux (t_1, t_2) and a steady-state phase of execution where output pixels have settled (t_3). The result is obtained by measuring the output pixels at steady-state.

2.1 CNN Edge Detector with Mismatched Analog Circuit

Cellular nonlinear networks are efficiently implementable with analog hardware as demonstrated in previous studies [16, 20]. These analog accelerators directly implement the CNN differential equations by leveraging the physics of the underlying circuits. Because circuits are subject to a range of nonidealities, the behavior of the CNN in hardware may deviate substantially from its expected behavior.

Device mismatch is one such nonideality that has been shown to degrade CNN convergence and edge detection quality in prior works [22, 71]. Mismatch occurs when analog hardware experiences random variations during fabrication, which prevent precise control of parameter values and cause identically configured values to deviate slightly between devices [37]. In CNN’s context, mismatch causes deviations in the programmed parameters A, B , and z , making every cell to undergo a slightly different dynamics as shown in Figure 2a where the δ random variables modeling the mismatch.

Figure 2b shows the time evolution of the CNN edge detector when device mismatch is applied to the A, B , and z parameters. In the mismatched CNN edge detector, the parameters are drawn from normal distributions centered around the nominal parameter values, with a relative standard deviation of 10% of the nominal value. That is, δ are drawn from $\mathcal{N}(1, 0.1)$. This statistical model is commonly used in design to assess the effect of mismatch on the system. Observe that the final output (t_3) is much noisier and significantly diverges from the ideal edge detection outcome presented in Figure 1c. This deviation in behavior occurs because the edge detector template design does not take mismatch into account [11, 12, 20, 44]. *Can we learn templates for the CNN edge detector that are resilient to device mismatch?*

2.2 Learning a Mismatch-Aware CNN Edge Detector

We want to learn a set of CNN parameters that minimize the mean-square error (MSE) between the reference edge detector output Y and the mismatched CNN output at time t_3 . The following cost function calculates the MSE of pixels between the reference output and output measured from the CNN at time t_3 :

$$\text{MSE}(Y, A, B, z) = \frac{1}{N} \sum_{ij} (y_{ij} - f(x_{ij}[A, B, z](t_3)))^2. \quad (1)$$

Because we want to learn a template resilient to mismatch that robustly performs the edge detection task, we want to minimize the *expected* mean-squared error over samples of random mismatch δ (Figure 2a). Therefore, the loss function for the mismatch-aware CNN edge detector is

$$\text{Loss}(Y, A, B, z) = \mathbb{E}_{\delta} [\text{MSE}(Y, A, B, z)]. \quad (2)$$

Designers would like to find a set of A , B , and z that minimizes this expected loss.

Challenges. Minimizing this loss function is highly non-trivial. Designers may attempt to analytically calculate a closed-form solution for the CNN’s output $f(x_{ij}(t_3))$ to avoid using a differential equation solver entirely. In the case of linear systems, this is possible, but because this system of differential equations is nonlinear, a closed-form solution cannot be easily derived analytically from the differential equations. Even for the CNN, a relatively simple nonlinear dynamical system, analysis is challenging [12]. These challenges are further complicated by random mismatches which introduce unpredictable deviations from the ideal behavior.

2.3 Mismatch-Aware CNN Edge Detection with Shem.

We present Shem, a framework that enables the gradient-based optimization of analog computations in the presence of hardware nonidealities. Shem supports direct optimization over the time-domain differential equation models of the analog system, enabling optimization over nonlinear dynamical systems that may exhibit stochastic behavior.

Shem works with a *tunable* differential equation model of the dynamical system and a cost function defined over the dynamical system’s state variable trajectories. Figure 3a presents the experimental setup for optimizing the mismatched CNN, written in Shem’s API.

Parameters. Shem allows annotation of the “trainable” parameters in the computation. The trainable parameters are those that designers want the optimizer to tune. We leverage the rotation invariance of an edge, leading to symmetric A and B templates to constrain the search space. Lines 2-4 instantiate trainable corner, edge, and center parameters, and Lines 5-7 construct the A template from these parameters. Lines 8-14 do the same for the B template and z . With these constraints, the optimizer tunes a total of 7 parameters. The Shem API accepts the CNN differential equations and compiles to a differentiable model in Line 19.

Cost Function. Figure 3b outlines the optimization setup. The cost function is defined in Lines 1-7. The model set the input u with an image and solves the differential equations in the time domain with sampled random mismatches. The MSE loss is computed over the model readout with a reference

```

1 def create_cnn_model(n_row, n_col):
2     A_corner = mismatch(AnalogTrainable(init=0), sigma=0.1)
3     A_edge = mismatch(AnalogTrainable(init=0), sigma=0.1)
4     A_center = mismatch(AnalogTrainable(init=2), sigma=0.1)
5     A = [[A_corner, A_edge, A_corner],
6          [A_edge, A_center, A_edge],
7          [A_corner, A_edge, A_corner]]
8     B_corner = mismatch(AnalogTrainable(init=-1), sigma=0.1)
9     B_edge = mismatch(AnalogTrainable(init=-1), sigma=0.1)
10    B_center = mismatch(AnalogTrainable(init=8), sigma=0.1)
11    B = [[B_corner, B_edge, B_corner],
12         [B_edge, B_center, B_edge],
13         [B_corner, B_edge, B_corner]]
14    z = mismatch(AnalogTrainable(init=-0.5), sigma=0.1)
15    # build the CNN dynamical system model
16    cnn_model = build_cnn_sys(dimension=(n_row, n_col),
17                             parameters=(A, B, z))
18    # Compile to a differentiable model
19    cnn_diff_model = Shem.compile(cnn_model)
20    return cnn_diff_model

```

(a) Trainable CNN Model Instantiation

```

1 def forward_evaluate(model, img, ref_edge_img):
2     model.set_param(model.U, img) # initialize input
3     # sample device mismatch with a seed
4     # and solve the differential equations
5     model.diffeq_solve(mismatch_sample_seed=new_seed())
6     cnn_edge_img = model.get_output()
7     return mse(cnn_edge_img, ref_edge_img)
8
9 # prepare input and edge images
10 training_set = Silhouettes(batch_size=128)
11 model = create_cnn_model(n_row=16, n_col=16)
12 model.set_readout_time([t3])
13 optimizer = Adam(lr=0.1)
14 for batch in training_set:
15     losses = []
16     for img, ref_edge_img in batch:
17         losses.append(forward_evaluate(model,
18                                     cnn_edge_img, ref_edge_img))
19     loss = mean(losses) # expected mse loss
20     grad = model.gradient(loss)
21     optimizer.update(model.trainables, grad)
22 return model.trainables

```

(b) CNN Edge Detection Optimization Setup. In practice, the for-loop in Lines 16-18 is executed in a vectorized form.

Figure 3. Simplified Shem Code Snippets.

edge image. The main optimization loop repeats the cost function to calculate the expected MSE.

Optimization Loop. Line 10 prepares the training set from the Caltech Silhouettes dataset, which provides 16×16 black-and-white images [53]. We set the batch size to 128. A differentiable CNN model is instantiated in Lines 11-12 with a specified readout time t_3 . The Adam optimizer, initialized with a learning rate of 0.1, is invoked in Line 13 to enable gradient-based updates [38]. The loop in Lines 14-21 processes the dataset (over 64 steps). MSE losses are computed over each image and its corresponding reference edge (Lines

17-18), and these individual losses are averaged at the end of each batch to obtain the expected MSE loss (Line 19). Based on this loss, Lines 20-21 compute the gradient, allowing the Adam optimizer to adjust the model’s trainable weights via gradient descent.

Results. The optimizer takes a total of 33 minutes on an Intel(R) Xeon(R) Silver 4216 CPU with a Quadro RTX 6000 GPU, totaling 31 seconds per iteration, and optimizes a non-linear differential equation system containing 256 differential equations over 128 simulations at each iteration. The MSE losses over optimization iterations are shown in Figure 2d.

Figure 2c shows the operation of the mismatched-optimized edge detector on the example image after 64 iterations of the gradient descent algorithm, and Figure 2e presents the learned parameters. As we can see after optimization, the final output image looks much cleaner, even though there is a large amount of mismatch in the system. We verified the learned templates on the testing set of the Caltech Silhouettes dataset with distinct random seeds. The optimizer achieves an MSE loss of 0.027 compared to 0.130 from the initial parameters. The results show how Shem’s differentiable formulation of the analog system enables the optimization of the CNN edge detector to be robust to device mismatch.

3 Time-Domain Optimization of Analog Systems

It is crucial that both analog computation and hardware non-idealities can be represented in differentiable forms. This allows for nonideality-aware optimization using gradient-based methods. In this section, we describe how analog computation can be modeled in a differentiable manner, with techniques from machine learning and scientific computing [8, 27, 31, 36, 46].

3.1 Optimization Problem

Analog computation can be modeled as a system of ordinary differential equations (ODEs) in the form

$$\frac{d\mathbf{x}(t)}{dt} = f(\mathbf{x}(t), \boldsymbol{\theta}, t), \quad (3)$$

where $\mathbf{x}(t) \in \mathbb{R}^n$ represents the state variables at time t with initial condition $\mathbf{x}(0) = \mathbf{x}_0$. $\boldsymbol{\theta} \in \mathbb{R}^m$ denotes the model parameters. $f : \mathbb{R}^n \times \mathbb{R}^m \times \mathbb{R} \rightarrow \mathbb{R}^n$ is the time derivative function of \mathbf{x} and is assumed to be differentiable with respect to both \mathbf{x} and $\boldsymbol{\theta}$. We consider a loss function $\mathcal{L} = \mathcal{L}(\mathbf{x}(t_0), \dots, \mathbf{x}(t_k))$ evaluated with the state variables observed at time t_0, \dots, t_k .

Gradient Computation. We seek to compute the gradient $\frac{d\mathcal{L}}{d\boldsymbol{\theta}}$ with respect to the system parameters $\boldsymbol{\theta}$, so that we can apply gradient descent-based approaches to optimize the loss function \mathcal{L} . This quantity is also referred to as sensitivity in literature [27]. Computing the gradient involves tracking the parameters’ effect throughout the dynamical system’s time evolution and can be obtained with two methods:

- *Backpropagation through Solver* Autodifferentiate a differential equation solver to obtain the gradient with respect to the parameters. More memory intensive.
- *Solving the Continuous Adjoint Equations* Augment the dynamical system with *adjoint* differential equations whose solution is the gradient. More compute intensive.

3.2 Backpropagation through the Solver

The first approach is to compute the gradient with backpropagation, similar to in a neural network, leveraging the differentiability of numerical ODE solvers. Numerical solvers compute the ODE solution in discrete time steps $\mathbf{x}_{\tau_0}, \mathbf{x}_{\tau_1}, \dots, \mathbf{x}_{\tau_N}$, where $\tau_N = t_k$. The state variable at time τ_i is calculated from the previous state(s) and the derivative function, for example, with Euler’s method.

$$\mathbf{x}_{\tau_{i+1}} = \mathbf{x}_{\tau_i} + \Delta t \cdot f(\mathbf{x}_{\tau_i}, \boldsymbol{\theta}, \tau_i), \quad (4)$$

where Δt is the time step size. Since f and the update operators are differentiable, $\mathbf{x}_{\tau_{i+1}}$ remain differentiable with respect to previous state \mathbf{x}_{τ_i} and $\boldsymbol{\theta}$. Therefore, we can apply backpropagation through the solver to compute $\frac{d\mathcal{L}}{d\boldsymbol{\theta}}$ with

$$\begin{aligned} \frac{d\mathcal{L}}{d\boldsymbol{\theta}} &= \frac{\partial \mathcal{L}}{\partial \mathbf{x}_{\tau_N}} \top \left(\frac{\partial \mathbf{x}_{\tau_N}}{\partial \mathbf{x}_{\tau_{N-1}}} \frac{d\mathbf{x}_{\tau_{N-1}}}{d\boldsymbol{\theta}} + \frac{\partial \mathbf{x}_{\tau_N}}{\partial \boldsymbol{\theta}} \right) \\ &= \frac{\partial \mathcal{L}}{\partial \mathbf{x}_{\tau_N}} \top \left(\frac{\partial \mathbf{x}_{\tau_N}}{\partial \mathbf{x}_{\tau_{N-1}}} \left(\frac{\partial \mathbf{x}_{\tau_{N-1}}}{\partial \mathbf{x}_{\tau_{N-2}}} \frac{d\mathbf{x}_{\tau_{N-2}}}{d\boldsymbol{\theta}} + \frac{\partial \mathbf{x}_{\tau_{N-1}}}{\partial \boldsymbol{\theta}} \right) + \frac{\partial \mathbf{x}_{\tau_N}}{\partial \boldsymbol{\theta}} \right) \quad (5) \\ &\dots \end{aligned}$$

Higher-order methods such as the Runge-Kutta method use more previous states to calculate $\mathbf{x}_{t_{au_{i+1}}}$ for better accuracy, and the operations still preserve differentiability.

This method is straightforward and efficient with modern automatic differentiation (AD) tools [5, 31, 36]. The downside is that it can be computationally expensive in terms of memory, as intermediate states and their corresponding gradients need to be stored to compute the loss gradients and scales with the number of time steps.

3.3 Solving the Continuous Adjoint Equations

The continuous adjoint method formulates the gradient computation as solving an augmented ODE system, which reduces memory usage by avoiding the need to store all intermediate states [8, 36, 50]. The adjoint is defined as $\mathbf{a}(t) \equiv \frac{\partial \mathcal{L}}{\partial \mathbf{x}(t)}$ and calculates the gradient with the following system of augmented ODEs:

$$\begin{cases} \frac{d\mathbf{x}(t)}{dt} = f(\mathbf{x}(t), \boldsymbol{\theta}, t), & \mathbf{x}(t_k) = \mathbf{x}_{t_k}, \\ \frac{d\mathbf{a}(t)}{dt} = -\mathbf{a}(t) \top \frac{\partial f(\mathbf{x}(t), \boldsymbol{\theta}, t)}{\partial \mathbf{x}(t)}, & \mathbf{a}(t_k) = \frac{\partial \mathcal{L}}{\partial \mathbf{x}(t_k)}, \\ \frac{d\mathbf{u}(t)}{dt} = -\mathbf{a}(t) \top \frac{\partial f(\mathbf{x}(t), \boldsymbol{\theta}, t)}{\partial \boldsymbol{\theta}}, & \mathbf{u}(t_k) = 0. \end{cases} \quad (6)$$

Here, $\mathbf{u}(0)$ will represent the gradient of interest, $\frac{d\mathcal{L}}{d\boldsymbol{\theta}}$. (For a detailed derivation, readers can refer to [8, 36]). The initial conditions are set to the state value at the end time t_k , which

is computed during the forward pass. To obtain $\mathbf{u}(0)$, we solve the augmented ODEs backward in time, i.e., from t_k to 0. All state variables in the augmented systems are computed on the fly, thus making the memory complexity independent of the number of time steps.

The key advantage of using the continuous adjoint method is its memory efficiency. However, this approach has drawbacks, including increased runtime and susceptibility to numerical error due to the additional ODE solving. Furthermore, the augmented system may exhibit instability. Therefore, the choice of technique should depend on the characteristics of the specific ODE being solved [36, 50].

4 Differentiable Modeling of Nonidealities

In the basic problem setup, $f(\mathbf{x}(t), \boldsymbol{\theta}, t)$ is assumed to be differentiable. In practice, analog nonidealities introduce stochastic and non-differentiable behaviors into the dynamics. In addition, digitally programmable elements (e.g., digital/analog converters) and measurement circuits discretize continuous signals, introducing discontinuities. We now extend the basic time-domain gradient calculation method to support common hardware nonidealities.

4.1 Device Mismatch

In analog hardware, device parameters (such as transistor threshold voltages, transistor sizes, capacitance value, etc) can vary slightly due to manufacturing variations. This device mismatch leads to deviations in the behavior of components between identical hardware units [37].

In the presence of device mismatch, the system dynamics are altered by perturbations $\boldsymbol{\delta}$ drawn from a probability distribution, typically $\mathcal{N}(1, \sigma^2 \cdot \mathbb{I})$, a multivariate normal distribution with unit mean and covariance $\sigma^2 \cdot \mathbb{I}$. For instance, mismatched can cause the ODE system to evolve with perturbed parameters $\boldsymbol{\theta}' = \boldsymbol{\delta} \circ \boldsymbol{\theta}$, e.g., Figure 2a. More generally, mismatches can multiply with any term in the derivative function f . Consequently, each realization of the ODE system with a different sample of $\boldsymbol{\delta}$ follows the dynamics

$$\frac{d\mathbf{x}(t)}{dt} = f_{\boldsymbol{\delta}}(\mathbf{x}(t), \boldsymbol{\theta}, t), \quad (7)$$

leading to a slightly different trajectory for the $\mathbf{x}(t)$ and variation in the loss function $\mathcal{L}_{\boldsymbol{\delta}}$. It is important to note that $\boldsymbol{\delta}$ is always a multiplicative term and thus does not affect the differentiability of the system. Hence, backpropagation and the continuous adjoint method remain applicable.

The loss gradient $\frac{d\mathcal{L}}{d\boldsymbol{\theta}}$ is calculated using Monte Carlo sampling, where multiple realizations of the mismatch vector $\boldsymbol{\delta}$ are drawn and the gradient $\frac{d\mathcal{L}_{\boldsymbol{\delta}}}{d\boldsymbol{\theta}}$ is computed for each realization. The final gradient is then obtained by averaging over all the Monte Carlo samples:

$$\frac{d\mathcal{L}}{d\boldsymbol{\theta}} = \mathbb{E}_{\boldsymbol{\delta}} \left[\frac{d\mathcal{L}_{\boldsymbol{\delta}}}{d\boldsymbol{\theta}} \right]. \quad (8)$$

4.2 Transient Noise

When the temperature is above absolute zero, the electrons in the devices move randomly, causing a tiny but unpredictable current which is called thermal noise. Thermal noise in the time domain is modeled as stochastic processes acting on the state variables over time, and the system dynamics are described by a stochastic differential equation (SDE) [36, 46]. Let $g : \mathbb{R}^n \times \mathbb{R}^m \times \mathbb{R} \rightarrow \mathbb{R}^{n \times q}$ be a deterministic function and differentiable with respect to \mathbf{x} and $\boldsymbol{\theta}$, a SDE is of the form

$$d\mathbf{x}(t) = f(\mathbf{x}(t), \boldsymbol{\theta}, t)dt + g(\mathbf{x}(t), \boldsymbol{\theta}, t)dW(t), \quad (9)$$

where $W(t)$ represents a q -dimensional Wiener process with prescribed correlation. This equation can be solved using numerical methods such as the Euler-Maruyama scheme, a variant of Euler's method with the update rule:

$$\mathbf{x}_{t_{i+1}} = \mathbf{x}_{t_i} + f(\mathbf{x}_{t_i}, \boldsymbol{\theta}, t_i)\Delta t + g(\mathbf{x}_{t_i}, \boldsymbol{\theta}, t_i)\boldsymbol{\xi}_{t_i}, \quad (10)$$

where $\boldsymbol{\xi}_{t_i}$ is an increment of the Wiener process which is essentially a multivariate normal distribution $\mathcal{N}(0, \Delta t \cdot \mathbb{I})$. Each SDE solve requires sampling $\boldsymbol{\xi}$ at every time point, leading to solution variations across different runs. Despite this inherent stochasticity, each solve behaves deterministically once a specific sample is drawn, and since the Euler-Maruyama scheme employs only differentiable operators, the process remains fully differentiable with respect to both $\boldsymbol{\theta}$ and \mathbf{x} , enabling backpropagation.

In the presence of transient noise, gradient computation can again be interpreted as a Monte Carlo simulation over noise samples. The gradient $\frac{d\mathcal{L}}{d\boldsymbol{\theta}}$ is averaged over samples:

$$\frac{d\mathcal{L}}{d\boldsymbol{\theta}} = \mathbb{E}_{\boldsymbol{\xi}} \left[\frac{d\mathcal{L}_{\boldsymbol{\xi}}}{d\boldsymbol{\theta}} \right]. \quad (11)$$

The continuous adjoint method is also applicable in the SDE setup with some modification [46].

Transient Noise and Mismatch. Since device mismatch is static, solving the system for a perturbation sample is no different from solving the non-mismatched ODE. Thus, incorporating both device mismatch and transient noise in the ODE is straightforward and can be done by adding multiplicative mismatch terms to the derivative (f) and the noise amplitude (g) functions. The gradient with both mismatch and noise can be computed using Monte Carlo sampling:

$$\frac{d\mathcal{L}}{d\boldsymbol{\theta}} = \mathbb{E}_{\boldsymbol{\delta}, \boldsymbol{\xi}} \left[\frac{d\mathcal{L}_{\boldsymbol{\delta}, \boldsymbol{\xi}}}{d\boldsymbol{\theta}} \right]. \quad (12)$$

This formulation enables a principled optimization of analog systems in the time domain through gradient descent while ensuring both device mismatch and transient noise are properly addressed.

4.3 Discrete Parameters

Analog hardware often implements configurable parameters in a quantized form because the control interface is

typically digital, such as switches or digital-to-analog converters (DACs), leading to discrete levels in parameter values. To incorporate such non-differentiable parameters into gradient-based optimization, one effective method is to use the Gumbel-Softmax estimator [33]. This method approximates the discrete distribution with a differentiable relaxation, enabling standard backpropagation, and is used in neural network architecture search, quantization-aware training, and physics-aware optical neural network [7, 33, 47].

Let $\theta_d \in \{p_1, p_2, \dots, p_k\}$ be a discrete parameter. The Gumbel-Softmax estimator introduces a relaxation $\hat{\theta}_d \approx \mathbf{y}^\top \mathbf{p}$, where $\mathbf{p} = [p_1, p_2, \dots, p_k]^\top$ is a vector of discrete levels. \mathbf{y} is a relaxed one-hot vector with each entry calculated as

$$y_i = \frac{\exp((\log(\pi_i) + g_i)/\tau)}{\sum_{j=1}^k \exp((\log(\pi_j) + g_j)/\tau)}, \quad (13)$$

where π_i is a learnable probability for the discrete level p_i , i.e., the larger the π_i , the more likely that $\hat{\theta}_d \approx p_i$. g_i is a small perturbation drawn from Gumbel(0, 1) distribution [33]. The temperature parameter τ controls the smoothness of the approximation: as $\tau \rightarrow \infty$, the distribution approaches a uniform distribution, while as $\tau \rightarrow 0$, \mathbf{y} becomes identical to a one-hot vector. Because $\frac{\partial \mathbf{y}}{\partial \pi}$ is well-defined, replacing non-differentiable discrete parameters with the Gumbel-Softmax estimator allows for the use of backpropagation. In practice, τ is annealed from high value to small but nonzero value with a linear schedule or an exponential decay schedule.

4.4 Bounded Parameters

In analog hardware, the parameter magnitudes vary widely due to differences in their physical characteristics. For example, capacitances may be at the pico scale and currents at the micro-scale. Therefore, normalization is critical to ensure stable and efficient gradient descent-based optimization. In practice, these parameters fall within physically reasonable ranges, allowing for normalization with the physical range followed by a clipping within certain limits, such as $[-1, 1]$.

5 Implementation of the Shem Framework

The Shem framework leverages the JAX ecosystem for implementing the differentiable analog system models with nonidealities [5]. Specifically, we utilize Difffrax, a JAX-based library specialized in solving differential equations that supports both backpropagation through the solver and the continuous adjoint method for ODEs and SDEs [36].

Shem’s analog modeling APIs are built on top of Ark, a programming language designed for defining analog compute paradigms [71]. Ark provides an expressive syntax for specifying analog compute models, which can be compiled into ODEs. By combining JAX’s high-performance automatic differentiation with Ark’s flexibility, Shem enables seamless optimization of complex analog systems.

5.1 Frontend APIs

Shem offers several core APIs to manage various aspects of analog systems, including noise, device mismatch, and discrete variables. These APIs integrate automatically with Difffrax’s ODE/SDE solvers and JAX’s autograd features:

- `AnalogTrainable` and `DiscreteTrainable`: The two classes represent trainable continuous and discrete parameters that will resolve to targets for gradient descent update.
- `mismatch`: This decorator introduces device mismatch into a trainable/non-trainable parameter. It adds a multiplicative symbolic mismatch term, which is concretized in execution time by drawing samples from a normal distribution with the provided relative standard deviation.
- `noiseexp`: This API allows for the specification of a noise amplitude function similar to defining a derivative function in Ark and Shem automatically adds to the system’s ODEs to form SDEs, as Ark does not provide SDE support.

5.2 Compilation to Differentiable Functions

Based on the provided specifications, Shem compiles the model into a differentiable function within the JAX framework. The forward pass solves the system of ODEs (or SDEs), while the backward pass computes gradients of the loss function with respect to the trainable parameters, using either backpropagation or the continuous adjoint method.

Once compiled as a differentiable function, the analog system can be optimized similarly to optimize a neural network. Users provide input-output data, random seeds for Monte Carlo sampling, and a loss function based on the system’s output versus the target output. Then, users can apply standard deep learning techniques for optimization, such as using the Adam optimizer for gradient descent, with GPU acceleration enabling large-scale parallelization [38].

5.3 Discussion

Modeling of Analog Hardware. Shem works with the differential equation representation of the underlying analog hardware, following the same design philosophy as Ark [71]. Shem’s ODE models operate at the same level of abstraction as behavioral, Simulink, and equivalent circuit models used in the early stages of circuit design. The parameterized ODEs produced by Shem serve as an executable requirements specification, constraining and informing the transistor-level unit cell designs, which would be developed with a fabrication-ready PDK. With this modeling approach, the ODE models are expected to be iteratively refined to capture more non-idealities at a finer granularity as the transistor-level designs are developed. The parameter constraints limit the ODE model to only allow reasonable parameterizations.

6 Case Studies

We use Shem in two design case studies to maximize an end-to-end application-specific quality metric. The case study

statistics and optimizer runtimes are summarized in Table 1. To our knowledge, this is the first work demonstrating the optimization of these systems in the presence of non-idealities. All experiments were conducted on an Intel(R) Xeon(R) Silver 4216 CPU paired with a Quadro RTX 6000 GPU.

6.1 Oscillator-Based Pattern Recognizer

In recent years, OBC has been used to solve combinatorial optimization problems energy efficiently and perform pattern recognition [9, 40, 51, 52, 58, 67]. In oscillator-based computing, information is encoded in the phase of an oscillating signal instead of traditional voltage or current levels. To perform computation, oscillators are coupled together; coupled oscillators will tend to synchronize so that they are either in-phase or out-of-phase. The ideal phase dynamics of the oscillators in OBC are captured with the *Kuramoto model*, a nonlinear differential equation [58, 70]:

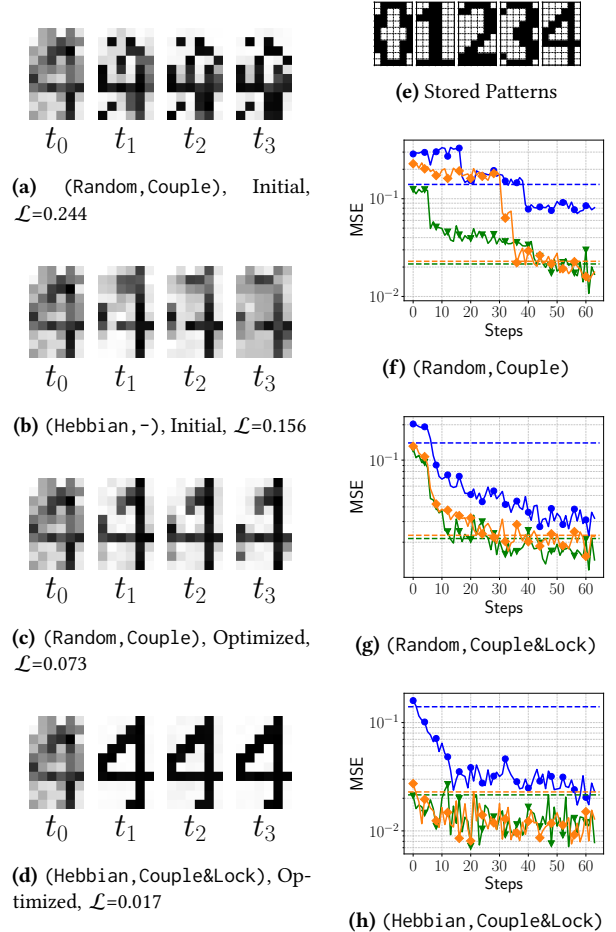
$$\frac{dx_i}{dt} = - \sum_{j=1}^n k_{ij} \sin(\pi(x_i - x_j)) - l \sin(2\pi x_i), i = 1, \dots, n. \quad (14)$$

The x_i state variables model the phase of oscillator i over time normalized by π , while the $k_{ij} \cdot \sin(\pi(x_i - x_j))$ term characterizes the interaction between oscillators i and j with coupling weight k_{ij} . On measurement, we center the phase to lie between $[0, 1]$. The more positive the coupling weight, the stronger the tendency for the two oscillators to synchronize in phase. Conversely, the more negative the coupling weight, the stronger the tendency for the oscillators to settle into distinct phases. The injection locking weight l controls the convergence speed [51, 58, 70].

Pattern Recognition. Networks of oscillators can “memorize” patterns and recover them from noisy inputs [40, 51, 67]. We parameterize the network to memorize five digits, each represented as a 10×6 pixel grid with black (0) and white (1) pixels, where each pixel p_i is mapped to an oscillator x_i (Figure 4e). The patterns are programmed into the OBC by setting coupling weights k , and the locking weight l is determined through parameter sweeping in simulation [67].

The goal of the recognizer is to have the oscillator phases converge to the original pattern from a noisy greyscale image, where each pixel is in $[0, 1]$ (e.g., Figure 4d). Each oscillator’s phase ϕ is directly set to the corresponding noisy image’s pixel value v_i . The dynamical system then evolves over time and settles to the memorized pattern that is the closest match. To recover the rectified image from the oscillators’ phase, we simply measure the phase of each oscillator.

6.1.1 Optimization with Shem. In this case study, we use Shem to learn the coupling weights from the dataset while simultaneously considering the nonidealities and resource limitations in the hardware implementation. We compare the efficacy of the learned hardware-aware coupling weights



Initial Coupling	Hebbian	Random	Random	Hebbian
Trainables	-	Couple	Couple & Lock	Couple & Lock
Couple bit width	1	0.140	0.077	0.029
	2	0.022	0.019	0.017
	3	0.023	0.017	0.019

(i) MSE Loss Comparison after Optimization

Figure 4. OBC Pattern Recognizer. *Left:* dynamics of OBC with 1-bit weights on noisy “4” input. *Right:* Loss ■: 1-bit; ■: 2-bits; ■: 3-bits, y-axis: $\log(\text{MSE})$, x-axis: iteration, dotted: Hebbian rule loss. *Bottom.* Loss for different optimizer setups.

against a Hebbian rule-based approach, which deterministically computes coupling weights from the patterns to memorize and tunes the locking weight without considering nonidealities [40, 51, 67]. We describe the target hardware and then present our optimization results.

6.1.2 OBC Hardware. Hardware implementations of OBC are susceptible to transient phase noise, which causes deviations in oscillator dynamics captured in the Kuramoto model in Equation 14, potentially degrading pattern recognition accuracy [41]. This is typically modeled as white noise in

Compute Paradigm	Application	Modeled Hardware Characteristics	Trainable Parameters		# of state variables	Cost function	Optimization runtime
			physical meaning	#			
CNN	Edge detection	Device mismatch	Feedforward, feedback and bias magnitude	19	256	MSE	33 mins
OBC	Pattern recognition	Discrete parameters Transient noise	Coupling and locking weight	104 (+1)	60	MSE	4 mins
TLN	PUF	Device mismatch	Capacitance, inductance, transconductance values	25	514	$\overline{I2O}$	1.4 hrs

Table 1. Benchmark Characteristics and Optimizer Runtime.

the Kuramoto model [70]. In this study, we introduce phase noise with a standard deviation of $\alpha = 0.025$.

$$\frac{dx_i}{dt} = - \sum_{j=1}^n k_{ij} \sin(\pi(x_i - x_j)) - l \sin(2\pi x_i) + \alpha \xi_i(t), \quad (15)$$

where $\xi_i(t)$ is a Gaussian white noise process and α is the noise amplitude. While small relative to coupling and locking signals, noise introduces random phase perturbations that impair synchronization. Noise is typically not considered when selecting the coupling weights.

Limited Connectivity. We arrange the oscillators in a grid and limit our OBC hardware to only allow neighboring oscillators to be coupled together. We limit coupling to neighbors because supporting all-to-all coupling between oscillators significantly increases area usage. For example, within the same device technology and chip area, an all-to-all connection accommodates 30 oscillators, with most of the area consumed by routing [52], while a neighboring connection supports up to 560 oscillators [3]. Thus, for large-scale problems, a neighboring connection is preferable. Hardware connectivity limitations are typically not considered when designing the OBC application, and all-to-all connectivity is expected.

Discrete Coupling Weight. In practice, the coupling weights are digitally programmed with a digital-to-analog converter (DAC), where the DAC’s bit width controls its precision [56]. Because higher-precision DACs consume more area and energy, selecting the DAC with the smallest bit width is preferable. We note that typically, the effects of coupling weight discretization on the computation are not considered.

6.1.3 Evaluation. We use Shem to optimize the OBC paradigm for the pattern recognizer under transient noise, with trainable discrete coupling weights in a neighboring connection topology. We use a dataset containing 512 pairs of digit images, where each pair contains an ideal and a noisy image with uniform($-0.5, 0.5$) noise added. The loss is the MSE between the OBC image readout and ideal image at measurement time $t = 1$. Both the noisy image and transient noise are resampled at the start of each batch to avoid overfitting.

We execute the Adam optimizer with a learning rate of 0.1 for 64 steps and anneal the temperature of the Gumbel softmax exponentially from 10 to 1. We report the MSE of the lowest-training-loss parameter set on a test set of 8192 image

pairs. The Hebbian baseline quantizes the coupling weights obtained from the Hebbian rules to the nearest discrete value and discards all non-neighboring oscillator weights.

Analysis. We initially learned coupling weights for 1, 2, and 3-bit DACs with the locking weight initialized to one. We use (Initialization, Trainables) to denote each instantiation; the (Random, Couple) run starts from a random initialization and optimizes the coupling weights, for example. Figure 4a and 4b shows that both the initial random parameterization and Hebbian baseline struggle to recover the "4" digit, with the Hebbian baseline doing marginally better.

Figures 4f, 4g, and 4h track the MSE loss over 60 iterations for each instantiation. The loss steadily decreases for both Random and Hebbian as the optimizer finds better solutions. Figure 4i illustrates the MSE loss for different optimization setups, where learned coupling and locking parameters achieve MSE reductions of 0.03-0.117 compared to Hebbian rule initialization. After optimizing the coupling weights with a 1-bit DAC, the results shown in Figure 4c indicate an improvement, as the OBC recovers a greater portion of the "4" digit, though the solution remains suboptimal.

Introducing trainable locking yields better results, especially in the 1-bit DAC configuration, with the loss reduced by 0.048 compared to the coupling-only setup. However, for 2-bit and 3-bit DACs, the optimizer converges to similar losses. The (Hebbian, Couple&Lock) setup achieves the best performance across all configurations, indicating a good initial guess leads to better convergence, which is common in gradient-based optimization. Notably, the 1-bit optimized coupling and locking run achieves a comparable loss to the 3-bit Hebbian initialization. Figure 4d shows qualitatively that the 1-bit OBC can recover "4" with a 1-pixel error in a noisy setting. We therefore identify the following design tradeoff: For a resource-bounded system, 1-bit DACs are preferred with acceptable loss; Otherwise, 2-bit DACs offer lower loss. There is no advantage in using 3-bit DACs, as the loss doesn’t improve.

6.2 Transmission Line-Based Security Primitive

Transmission line-based computing (TLN) is an analog compute model that mimics the propagation of electromagnetic waves through transmission lines to perform computation [71]. The transmission lines are organized into a network, where

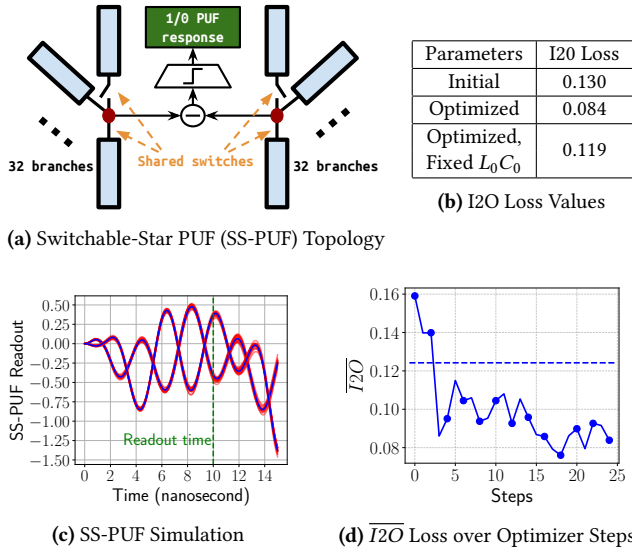


Figure 5. Transmission Line PUF. *Top-left.* Switchable-Star PUF. *Bottom-left.* Simulation of two mismatched designs: ■: mismatch only, ■: mismatch and noise. *Right.* optimizer loss

the reflection, transmission, and superposition of waves are used to perform computation. The system is modeled by the Telegrapher’s equations, discretized for the line segments:

$$\begin{cases} \frac{dV_i}{dt} = \frac{1}{C_i}(I_i - I_{i+1}), \\ \frac{dI_i}{dt} = \frac{1}{L_i}(V_{i-1} - V_i), \end{cases} \quad (16)$$

Here, V_i and I_i are the voltage and current at segment i , and L_i , and C_i are the inductance and capacitance parameters, respectively, and control propagation speed. With this paradigm, we are primarily interested in measuring the traveling wave on a particular link at the readout time *before* the system has settled. In contrast, most analog computing models only use the steady-state value.

TLN Hardware. The TLN model can be emulated with analog circuits typically used to implement filters. The hardware implementation introduces the scaling parameters $gc_{t,i}$, $gc_{s,i}$, $gl_{t,i}$, and $gl_{s,i}$ which map to lumped transistor parameters:

$$\begin{cases} \frac{dV_i}{dt} = \frac{1}{C_i}(gc_{t,i} \cdot I_i - gc_{s,i+1} \cdot I_{i+1}), \\ \frac{dI_i}{dt} = \frac{1}{L_i}(gl_{t,i-1} \cdot V_{i-1} - gl_{s,i} \cdot V_i). \end{cases} \quad (17)$$

Mismatch in these parameters causes deviations from the expected behavior, affecting the system’s transient dynamics.

6.2.1 TLN-based PUF. A Physical Unclonable Function (PUF) is a hardware security primitive that leverages intrinsic manufacturing variations to generate unique and unpredictable responses (output bits) for given challenges (input bits). For this application, we exploit rather than eliminate the effect of process variation and optimize the system to amplify the effect of mismatch on the dynamics of the

TLN [17, 71]. In this case study, we start with a 32-bit “Switchable Star” TLN PUF design (SS-PUF), pictured in Figure 5a. The SS-PUF has two nominally identical circuits (without mismatch), each with 32 switchable branches. Each branch is a transmission line controlled by a programmable switch that connects or disconnects the branch, where the switch is set by a challenge bit. During execution, a pulse is dispatched at the stars’ centers, and the response is measured by thresholding the signal difference of the center nodes at $t = 10$ nanoseconds. A positive signal is mapped to a “1” response bit. We use a logistic function to make the thresholding operation on readout differentiable.

Evaluation Metric. We optimize the $\overline{I2O}$ (mean instance-to-optimum) metric, a PUF security metric that measures the bias of the response bit over the space of similar challenges [65]. The intuition is that the response to a given challenge should not reveal information about the response to a slightly modified challenge; otherwise, a savvy attacker can exploit these correlations. Formally, $\overline{I2O}$ for r instances of a PUF design with n -bit challenges is defined as:

$$\overline{I2O} = \frac{1}{r} \sum_{i=1}^r \left(\frac{1}{n} \sum_{j=1}^n |S_j(P_i) - 0.5| \right), \quad (18)$$

where $S_j(P_i)$ represents the probability that flipping the j -th bit of a challenge for the i -th instance results in a flipped response, and n is the number of challenge bits. We observe this PUF metric is differentiable.

6.2.2 Optimization with Shem. We use Shem to optimize the gc , gl , L , and C parameters in the SS-PUF to minimize the $I2O$ loss. To the best of our knowledge, this is the first work to optimize PUF design parameters to minimize/maximize a security metric.

Experimental Setup. For the optimization process, we use eight mismatched parameter sets and 32 sets of similar challenges per batch, where each set contains 32 challenges that are one bit flip apart from a “reference” challenge. Both the mismatches and challenges are resampled in every batch to avoid overfitting. The system is optimized using the Adam optimizer with a learning rate of 0.005 for a total of 24 steps. All parameters are AnalogTrainable with initialization $C_i = L_i = 10^{-9}$ and $gc_{t,i} = gc_{s,i} = gl_{t,i} = gl_{s,i} = 1$, which produce the baseline $\overline{I2O} = 0.130$. We constrain each link in the SS-PUF to have the same parameter values; we learned from designing the SS-PUF that the response is more uniformly sensitive to mismatch if symmetry is preserved. For testing, we evaluate 192 mismatched PUFs with the same challenge setup as during training.

Analysis. Figure 5d shows the $I2O$ loss over optimization iterations. Fluctuations in the loss curve are expected due to the limited subspace of the PUF that is sampled during optimization (2^{10} out of the total 2^{32} challenge space). Despite these fluctuations, a clear overall trend of decreasing loss

is visible. This improvement remains consistent in testing, improving $\overline{I2O}$ from 0.130 to 0.089. Therefore, the optimized design improves statistical security properties of the design.

The optimized ODE produces TLN trajectories very sensitive to mismatch, but not chaotic. Figure 5c shows the noiseless (blue lines) and noisy (red lines) response of two mismatched SS-PUFs instances, where we inject white noise with a standard deviation of 1×10^{-7} estimated with a MOS transistor thermal noise model [61]. We observe the noisy trajectories closely follow the noiseless trajectory for the same instance, and the two mismatched instances produce very different trajectories. In a chaotic system, a very small perturbation from noise would produce a drastically different result in a chaotic system, rendering the PUF unstable.

With Shem, we can easily study the importance of certain parameters. We perform multiple optimization runs and observe one of the runs has difficulty reducing the loss. We compare the parameters and find that the failing run chooses very different center node capacitance C_0 and inductance L_0 values from the succeeding runs. We hypothesize the center node parameters have an outsized effect on the $\overline{I2O}$ score and optimize the SS-PUF with non-trainable C_0, L_0 . With these two parameters fixed, Shem achieves a loss of 0.119 compared to 0.084, indicating the C_0, L_0 parameters have an outsized effect on the security properties of the PUF.

7 Related Work

Analog EDA Tools. The “adjoint sensitivity analysis” technique in analog design automation originated in the late 1960s, and has since been expanded by numerous studies, including [13, 14, 19, 34, 62, 69]. These works focus on device-level optimization, specializing in circuit-specific metrics such as delay or gain. Our approach works with higher-level ODE models, optimizing end-to-end system-level cost functions. Additionally, we support nonidealities and digital control logic, which is crucial for mixed-signal design.

Adjoint Method for Design Optimization. The adjoint method is extensively used in the inverse design, as discussed in [25, 43]. For example, in the inverse design of photonic devices, they perform a forward simulation of the Maxwell’s equation with the finite-difference frequency-domain (FDFD) or finite-difference time-domain (FDTD) method and solve the adjoint with a backward simulation [21, 30, 55, 66]. Their framework targets Maxwell’s equations, a specific partial differential equation model, to model the electromagnetic dynamics of photonic devices. We model general ordinary differential equations with first-class support of nonidealities common in unconventional analog systems.

Physics-Aware Training. Practitioners have developed physics-aware training algorithms for ML pipelines used for in-sensor compression and machine vision, diffractive optical neural networks for image classification, and deep physical neural network [47–49, 73]. They implement some

or all parts of the neural network with their hardware platform and utilize differentiable hardware models to include physical behaviors or nonidealities during training. The modeling process is sophisticated and manually done in a per-hardware manner. Our work complements this area of research by introducing a framework that enables a systematic description of analog computing paradigms and their compilation into differentiable models, simplifying the modeling process in physics-aware training. Moreover, our framework extends beyond neural network training and supports the general optimization of unconventional analog systems.

Physics-Informed Neural Network A physics-informed neural network (PINN) integrates physical laws into its loss function to guide the learning process and has applications in solving forward and inverse problems in fluid dynamics, geoscience, material design, etc. [6, 18]. In contrast, our approach directly simulates systems, ensuring that the underlying dynamics are faithfully captured by construction rather than approximated by a trained neural network. These methods are complementary – when parts of an analog system are too complex to model directly, they can be represented using a PINN, and since both approaches are differentiable, the entire system can be optimized end-to-end.

Neural Differential Equations. Neural differential equations (NDEs) use neural networks to model state variable derivatives and have applications in generative models, dynamical systems, and time series prediction [8, 36, 46]. In contrast, our approach directly computes the physical dynamics in analog computations. Interestingly, analog computing, which naturally solves differential equations, is well-suited for NDE hardware, as suggested by [72]. Our framework provides a flexible tool for exploring and designing analog circuits to support NDE implementations.

8 Conclusion

We presented Shem, an optimization framework for analog systems with support for key analog hardware characteristics, including device mismatch, noise, and discreteness. Shem leverages differentiation methods recently popularized to train neural ODEs to enable optimization of analog systems and is built on the JAX ML framework, inheriting the programming conveniences and performance optimizations from the library. We demonstrated that Shem optimizes unconventional analog systems in the presence of hardware nonidealities that have not been optimized with automated methods previously. We view Shem as the initial step to connecting the two domains, enabling the application of optimization and gradient-based methods typically reserved for training neural ODEs to optimize analog hardware.

References

- [1] The Decadal Plan for Semiconductors, A Pivotal Roadmap Outlining Research Priorities. <https://www.src.org/about/decadal-plan>. Accessed: 2022-11-10.

- [2] Sara Achour and Martin Rinard. Noise-aware Dynamical System Compilation for Analog Devices with Legno. In *Proceedings of the Twenty-Fifth International Conference on Architectural Support for Programming Languages and Operating Systems*, pages 149–166, 2020.
- [3] Ibrahim Ahmed, Po-Wei Chiu, William Moy, and Chris H Kim. A Probabilistic Compute Fabric Based on Coupled Ring Oscillators for Solving Combinatorial Optimization Problems. *IEEE Journal of Solid-State Circuits*, 56(9):2870–2880, 2021.
- [4] Andreas Bayerstadler, Guillaume Becquin, Julia Binder, Thierry Botter, Hans Ehm, Thomas Ehmer, Marvin Erdmann, Norbert Gaus, Philipp Harbach, Maximilian Hess, et al. Industry Quantum Computing Applications. *EPJ Quantum Technology*, 8(1):25, 2021.
- [5] James Bradbury, Roy Frostig, Peter Hawkins, Matthew James Johnson, Chris Leary, Dougal Maclaurin, George Necula, Adam Paszke, Jake VanderPlas, Skye Wanderman-Milne, and Qiao Zhang. JAX: Composable Transformations of Python+NumPy Programs, 2018.
- [6] Shengze Cai, Zhiping Mao, Zhicheng Wang, Minglang Yin, and George Em Karniadakis. Physics-Informed Neural Networks (PINNs) for Fluid Mechanics: A Review. *Acta Mechanica Sinica*, 37(12):1727–1738, 2021.
- [7] Jianlong Chang, Yiwen Guo, Gaofeng Meng, Shiming Xiang, Chunhong Pan, et al. Data: Differentiable Architecture Approximation. *Advances in Neural Information Processing Systems*, 32, 2019.
- [8] Ricky TQ Chen, Yulia Rubanova, Jesse Bettencourt, and David K Duvenaud. Neural Ordinary Differential Equations. *Advances in neural information processing systems*, 31, 2018.
- [9] Jeffrey Chou, Suraj Bramhavar, Siddhartha Ghosh, and William Herzog. Analog Coupled Oscillator Based Weighted Ising Machine. *Scientific reports*, 9(1):14786, 2019.
- [10] Leon O Chua, Martin Hasler, George S Moschytz, and Jacques Neiryneck. Autonomous Cellular Neural Networks: a Unified Paradigm for Pattern Formation and Active Wave Propagation. *IEEE Transactions on Circuits and Systems I: Fundamental theory and applications*, 42(10):559–577, 1995.
- [11] Leon O Chua and Lin Yang. Cellular Neural Networks: Applications. *IEEE Transactions on circuits and systems*, 35(10):1273–1290, 1988.
- [12] Leon O Chua and Lin Yang. Cellular Neural Networks: Theory. *IEEE Transactions on circuits and systems*, 35(10):1257–1272, 1988.
- [13] Andrew R Conn, Paula K Coulman, Ruud A Haring, Gregory L Morrill, Chandramouli Visweswariah, and Chai Wah Wu. Jiffytune: Circuit Optimization Using Time-domain Sensitivities. *IEEE Transactions on Computer-Aided Design of Integrated Circuits and Systems*, 17(12):1292–1309, 1998.
- [14] Andrew R Conn, Ibrahim M Elfadel, WW Molzen Jr, PR O’Brien, Philip N Strenski, Chandramouli Visweswariah, and CB Whan. Gradient-based Optimization of Custom Circuits Using a Static-timing Formulation. In *Proceedings of the 36th annual ACM/IEEE Design Automation Conference*, pages 452–459, 1999.
- [15] Glenn ER Cowan, Robert C Melville, and Yannis P Tsividis. A VLSI Analog Computer/digital Computer Accelerator. *IEEE Journal of Solid-State Circuits*, 41(1):42–53, 2005.
- [16] JM Cruz and LO Chua. A 16×16 Cellular Neural Network Universal Chip: The First Complete Single-chip Dynamic Computer Array with Distributed Memory and with Gray-scale Input-output. *Analog Integrated Circuits and Signal Processing*, 15:227–237, 1998.
- [17] György Csaba, Xueming Ju, Qingqing Chen, Wolfgang Porod, Jürgen Schmidhuber, Ulf Schlichtmann, Paolo Lugli, and Ulrich Rührmar. On-chip Electric Waves: An Analog Circuit Approach to Physical Uncloneable Functions. *Cryptology ePrint Archive*, 2009.
- [18] Salvatore Cuomo, Vincenzo Schiano Di Cola, Fabio Giampaolo, Gianluigi Rozza, Maziar Raissi, and Francesco Piccialli. Scientific Machine Learning through Physics-Informed Neural Networks: Where We Are and What’s Next. *Journal of Scientific Computing*, 92(3):88, 2022.
- [19] Stephen Director and Ronald Rohrer. The Generalized Adjoint Network and Network Sensitivities. *IEEE Transactions on Circuit Theory*, 16(3):318–323, 1969.
- [20] Shukai Duan, Xiaofang Hu, Zhekang Dong, Lidan Wang, and Pinaki Mazumder. Memristor-based Cellular Nonlinear/neural Network: Design, Analysis, and Applications. *IEEE transactions on neural networks and learning systems*, 26(6):1202–1213, 2014.
- [21] Yuriy Elesin, Boyan Stefanov Lazarov, Jakob Søndergaard Jensen, and Ole Sigmund. Time Domain Topology Optimization of 3d Nanophotonic Devices. *Photonics and Nanostructures-Fundamentals and Applications*, 12(1):23–33, 2014.
- [22] Jorge Fernández-Berni and Ricardo Carmona-Galán. On the Implementation of Linear Diffusion in Transconductance-based Cellular Nonlinear Networks. *International Journal of Circuit Theory and Applications*, 37(4):543–567, 2009.
- [23] Luigi Fortuna, Paolo Arena, David Balya, and Akos Zarandy. Cellular Neural Networks: a Paradigm for Nonlinear Spatio-temporal Processing. *IEEE Circuits and Systems magazine*, 1(4):6–21, 2001.
- [24] Daibashish Gangopadhyay, Emily G Allstot, Anna MR Dixon, Karthik Natarajan, Subhanshu Gupta, and David J Allstot. Compressed Sensing Analog Front-end for Bio-sensor Applications. *IEEE Journal of Solid-State Circuits*, 49(2):426–438, 2014.
- [25] Dan Givoli. A Tutorial on the Adjoint Method for Inverse Problems. *Computer Methods in Applied Mechanics and Engineering*, 380:113810, 2021.
- [26] Ning Guo, Yipeng Huang, Tao Mai, Sharvil Patil, Chi Cao, Mingoo Seok, Simha Sethumadhavan, and Yannis Tsividis. Energy-efficient Hybrid Analog/digital Approximate Computation in Continuous Time. *IEEE Journal of Solid-State Circuits*, 51(7):1514–1524, 2016.
- [27] Alan C. Hindmarsh, Peter N. Brown, Keith E. Grant, Steven L. Lee, Radu Serban, Dan E. Shumaker, and Carol S. Woodward. SUNDIALS: Suite of Nonlinear and Differential/Algebraic Equation Solvers. *ACM Trans. Math. Softw.*, 31(3):363–396, September 2005.
- [28] Wenfei Hu, Zuochang Ye, and Yan Wang. Adjoint Transient Sensitivity Analysis for Objective Functions Associated to Many Time Points. In *2020 57th ACM/IEEE Design Automation Conference (DAC)*, pages 1–6. IEEE, 2020.
- [29] Yipeng Huang, Ning Guo, Mingoo Seok, Yannis Tsividis, Kyle Mandli, and Simha Sethumadhavan. Hybrid Analog-digital Solution of Non-linear Partial Differential Equations. In *2017 50th Annual IEEE/ACM International Symposium on Microarchitecture (MICRO)*, pages 665–678. IEEE, 2017.
- [30] Tyler W Hughes, Momchil Minkov, Ian AD Williamson, and Shanhui Fan. Adjoint Method and Inverse Design for Nonlinear Nanophotonic Devices. *ACS Photonics*, 5(12):4781–4787, 2018.
- [31] Mike Innes, Alan Edelman, Keno Fischer, Chris Rackauckas, Elliot Saba, Viral B Shah, and Will Tebbutt. A Differentiable Programming System to Bridge Machine Learning and Scientific Computing. *arXiv preprint arXiv:1907.07587*, 2019.
- [32] Mihai Irimia-Vladu, Eric D Glowacki, Gundula Voss, Siegfried Bauer, and Niyazi Serdar Sariciftci. Green and Biodegradable Electronics. *Materials Today*, 15(7-8):340–346, 2012.
- [33] Eric Jang, Shixiang Gu, and Ben Poole. Categorical Reparameterization with Gumbel-Softmax. *arXiv preprint arXiv:1611.01144*, 2016.
- [34] Deepak Joshi, Satyabrata Dash, HS Jatana, Ratnajit Bhattacharjee, and Gaurav Trivedi. Analog Circuit Optimization Using Adjoint Network Based Sensitivity Analysis. *AEU-International Journal of Electronics and Communications*, 82:221–225, 2017.
- [35] Chanik Kang, Chaejin Park, Myunghoo Lee, Joonho Kang, Min Seok Jang, and Haejun Chung. Large-scale photonic inverse design: computational challenges and breakthroughs. *Nanophotonics*, (0), 2024.
- [36] Patrick Kidger. *On Neural Differential Equations*. PhD thesis, University of Oxford, 2021.

- [37] Peter R Kinget. Device Mismatch and Tradeoffs in the Design of Analog Circuits. *IEEE Journal of Solid-State Circuits*, 40(6):1212–1224, 2005.
- [38] Diederik P. Kingma and Jimmy Ba. Adam: A Method for Stochastic Optimization, 2017.
- [39] Saikrishna Reddy Konatham, Reza Maram, Luis Romero Cortés, Jun Ho Chang, Leslie Rusch, Sophie LaRoche, Hugues Guillet de Chatellus, and José Azaña. Real-time Gap-free Dynamic Waveform Spectral Analysis with Nanosecond Resolutions through Analog Signal Processing. *Nature communications*, 11(1):1–12, 2020.
- [40] Ankit Kumar and Pritiraj Mohanty. Autoassociative Memory and Pattern Recognition in Micromechanical Oscillator Network. *Scientific reports*, 7(1):411, 2017.
- [41] Thomas H Lee and Ali Hajimiri. Oscillator Phase Noise: A Tutorial. *IEEE journal of solid-state circuits*, 35(3):326–336, 2000.
- [42] J-R L equepeys, Marc Duranton, Susana Bonnetier, Sandrine Catrou, Richard Fournel, Thomas Ernst, Laurent H erault, D Louis, Ahmed Jerraya, Alexandre Valentian, et al. Overcoming the Data Deluge Challenges with Greener Electronics. In *ESSDERC 2021-IEEE 51st European Solid-State Device Research Conference (ESSDERC)*, pages 7–14. IEEE, 2021.
- [43] Leon Lettermann, Alejandro Jurado, Timo Betz, Florentin W org otter, and Sebastian Herzog. Tutorial: a Beginner’s Guide to Building a Representative Model of Dynamical Systems Using the Adjoint Method. *Communications Physics*, 7(1):128, 2024.
- [44] Huaqing Li, Xiaofeng Liao, Chuandong Li, Hongyu Huang, and Chaojie Li. Edge Detection of Noisy Images Based on Cellular Neural Networks. *Communications in Nonlinear Science and Numerical Simulation*, 16(9):3746–3759, 2011.
- [45] Jiahua Li, Danyal Ahsanullah, Zhengqi Gao, and Ron Rohrer. Circuit Theory of Time Domain Adjoint Sensitivity. *IEEE Transactions on Computer-Aided Design of Integrated Circuits and Systems*, 2023.
- [46] Xuechen Li, Ting-Kam Leonard Wong, Ricky TQ Chen, and David Duvenaud. Scalable Gradients for Stochastic Differential Equations. In *International Conference on Artificial Intelligence and Statistics*, pages 3870–3882. PMLR, 2020.
- [47] Yingjie Li, Ruiyang Chen, Weilu Gao, and Cunxi Yu. Physics-aware Differentiable Discrete Codesign for Diffractive Optical Neural Networks. In *Proceedings of the 41st IEEE/ACM International Conference on Computer-Aided Design*, pages 1–9, 2022.
- [48] Yingjie Li, Ruiyang Chen, Minhan Lou, Berardi Sensale-Rodriguez, Weilu Gao, and Cunxi Yu. Lightridge: An End-to-end Agile Design Framework for Diffractive Optical Neural Networks. In *Proceedings of the 28th ACM International Conference on Architectural Support for Programming Languages and Operating Systems, Volume 4*, pages 202–218, 2023.
- [49] Tianrui Ma, Adith Jagadish Bolor, Xiangxing Yang, Weidong Cao, Patrick Williams, Nan Sun, Ayan Chakrabarti, and Xuan Zhang. Leca: In-sensor Learned Compressive Acquisition for Efficient Machine Vision on the Edge. In *Proceedings of the 50th Annual International Symposium on Computer Architecture*, pages 1–14, 2023.
- [50] Yingbo Ma, Vaibhav Dixit, Mike Innes, Xingjian Guo, and Christopher Rackauckas. A Comparison of Automatic Differentiation and Continuous Sensitivity Analysis for Derivatives of Differential Equation Solutions, 2021.
- [51] Paolo Maffezzoni, Bichoy Bahr, Zheng Zhang, and Luca Daniel. Oscillator Array Models for Associative Memory and Pattern Recognition. *IEEE Transactions on Circuits and Systems I: Regular Papers*, 62(6):1591–1598, 2015.
- [52] Antik Mallick, Mohammad Khairul Bashar, Daniel S Truesdell, Benton H Calhoun, Siddharth Joshi, and Nikhil Shukla. Graph Coloring Using Coupled Oscillator-based Dynamical Systems. In *2021 IEEE International Symposium on Circuits and Systems (ISCAS)*, pages 1–5. IEEE, 2021.
- [53] Benjamin Marlin, Kevin Swersky, Bo Chen, and Nando Freitas. Inductive Principles for Restricted Boltzmann Machine Learning. In Yee Whye Teh and Mike Titterton, editors, *Proceedings of the Thirteenth International Conference on Artificial Intelligence and Statistics*, volume 9 of *Proceedings of Machine Learning Research*, pages 509–516, Chia Laguna Resort, Sardinia, Italy, 13–15 May 2010. PMLR.
- [54] Adnan Mehonic, Abu Sebastian, Bipin Rajendran, Osvaldo Simeone, Eleni Vasilaki, and Anthony J Kenyon. Memristors—from In-memory Computing, Deep Learning Acceleration, and Spiking Neural Networks to the Future of Neuromorphic and Bio-inspired Computing. *Advanced Intelligent Systems*, 2(11):2000085, 2020.
- [55] Sean Molesky, Zin Lin, Alexander Y Piggott, Weiliang Jin, Jelena Vuckovi c, and Alejandro W Rodriguez. Inverse Design in Nanophotonics. *Nature Photonics*, 12(11):659–670, 2018.
- [56] William Moy, Ibrahim Ahmed, Po-wei Chiu, John Moy, Sachin S Sapatnekar, and Chris H Kim. A 1,968-node Coupled Ring Oscillator Circuit for Combinatorial Optimization Problem Solving. *Nature Electronics*, 5(5):310–317, 2022.
- [57] Boris Murmann, Marian Verhelst, and Yiannos Manoli. Analog-to-information Conversion. *NANO-CHIPS 2030: On-Chip AI for an Efficient Data-Driven World*, pages 275–292, 2020.
- [58] Karlheinz Ochs, Bakr Al Beattie, and Sebastian Jenderny. An Ising Machine Solving Max-cut Problems Based on the Circuit Synthesis of the Phase Dynamics of a Modified Kuramoto Model. In *2021 IEEE International Midwest Symposium on Circuits and Systems (MWSCAS)*, pages 982–985. IEEE, 2021.
- [59] Carlos Outeiral, Martin Strahm, Jiye Shi, Garrett M Morris, Simon C Benjamin, and Charlotte M Deane. The Prospects of Quantum Computing in Computational Molecular Biology. *Wiley Interdisciplinary Reviews: Computational Molecular Science*, 11(1):e1481, 2021.
- [60] Alexander Y Piggott, Eric Y Ma, Logan Su, Geun Ho Ahn, Neil V Sapra, Dries Vercauysse, Andrew M Netherton, Akhilesh SP Khope, John E Bowers, and Jelena Vuckovic. Inverse-designed photonics for semiconductor foundries. *ACS Photonics*, 7(3):569–575, 2020.
- [61] Behzad Razavi. *Design of Analog CMOS Integrated Circuits*. McGraw-Hill, second edition, 2005.
- [62] RA Rohrer. Fully Automated Network Design by Digital Computer: Preliminary Considerations. *Proceedings of the IEEE*, 55(11):1929–1939, 1967.
- [63] Jussi Ryynanen, Kalle Kivekas, Jarkko Jussila, Aarno Parssinen, and Kari Al Halonen. A Dual-band Rf Front-end for Wcdma and Gsm Applications. *IEEE Journal of Solid-State Circuits*, 36(8):1198–1204, 2001.
- [64] Abu Sebastian, Manuel Le Gallo, Riduan Khaddam-Aljameh, and Evangelos Eleftheriou. Memory Devices and Applications for In-memory Computing. *Nature nanotechnology*, 15(7):529–544, 2020.
- [65] Wolfgang Stefani, Fynn Kappelhoff, Martin Gruber, Yu-Neng Wang, Sara Achour, Debdeep Mukhopadhyay, and Ulrich R uhrmair. Strong PUF Security Metrics: Sensitivity of Responses to Single Challenge Bit Flips. *Cryptology ePrint Archive, Paper 2024/378*, 2024.
- [66] Logan Su, Dries Vercauysse, Jinjie Skarda, Neil V Sapra, Jan A Petykiewicz, and Jelena Vuckovi c. Nanophotonic Inverse Design with Spins: Software Architecture and Practical Considerations. *Applied Physics Reviews*, 7(1), 2020.
- [67] Aida Todri-Sanial, Stefania Carapezzi, Corentin Delacour, Madeleine Abernot, Thierry Gil, Elisabetta Corti, Siegfried F Karg, Juan N u nez, Manuel Jim enez, Mar ia J Avedillo, et al. How Frequency Injection Locking Can Train Oscillatory Neural Networks to Compute in Phase. *IEEE transactions on neural networks and learning systems*, 33(5):1996–2009, 2021.
- [68] Yannis Tsvividis. Not Your Father’s Analog Computer. *IEEE Spectrum*, 55(2):38–43, 2018.
- [69] Chandu Visweswariah, Ruud A Haring, and Andrew R Conn. Noise Considerations in Circuit Optimization. *IEEE Transactions on*

- Computer-Aided Design of Integrated Circuits and Systems*, 19(6):679–690, 2000.
- [70] Tianshi Wang and Jaijeet Roychowdhury. Oscillator-based Ising Machine. *arXiv preprint arXiv:1709.08102*, 2017.
- [71] Yu-Neng Wang, Glenn Cowan, Ulrich Rührmair, and Sara Achour. Design of Novel Analog Compute Paradigms with Ark. In *Proceedings of the 29th ACM International Conference on Architectural Support for Programming Languages and Operating Systems, Volume 2*, pages 269–286, 2024.
- [72] Mohamed Watfa and Alberto Garcia-Ortiz. Adjoint method: The connection between analog-based equilibrium propagation architectures and neural ODEs. In *Machine Learning with New Compute Paradigms*, 2023.
- [73] Logan G Wright, Tatsuhiko Onodera, Martin M Stein, Tianyu Wang, Darren T Schachter, Zoey Hu, and Peter L McMahon. Deep Physical Neural Networks Trained with Backpropagation. *Nature*, 601(7894):549–555, 2022.